

Hyperglycemia compromises the ischemia-provoked dedifferentiation of cerebral pericytes through p21–SOX2 signaling in high-fat diet-induced murine model

Hao-Kuang Wang^{1,2}, Chih-Yuan Huang³, Yun-Wen Chen⁴
and Yuan-Ting Sun^{5,6} 

Diabetes & Vascular Disease Research
January-February 2021: 1–13
© The Author(s) 2021
Article reuse guidelines:
sagepub.com/journals-permissions
DOI: 10.1177/1479164121990641
journals.sagepub.com/home/dvr


Abstract

Aim: Diabetes-related cerebral small vessel disease (CSVD) causes neurological deficits. Patients with diabetes showed pericyte loss as a hallmark of retinopathy. Cerebral pericytes, which densely localize around brain capillaries, are quiescent stem cells regulating regeneration of brain and may have a role in CSVD development. This study investigated whether diabetes impairs ischemia-provoked dedifferentiation of pericytes.

Methods: A murine high-fat diet (HFD)-induced diabetes model was used. After cerebral ischemia induction in the mice, pericytes were isolated and grown for a sphere formation assay.

Results: The sphere counts from the HFD group were lower than those in the chow group. As the spheres formed, pericyte marker levels decreased and SOX2 levels increased gradually in the chow group, but not in the HFD group. Before sphere formation, pericytes from the HFD group showed high p21 levels. The use of a p21 inhibitor rescued the reduction of sphere counts in the HFD group. At cellular level, hyperglycemia-induced ROS increased the level of p21 in cerebral pericytes. The p21–SOX2 signaling was then activated after oxygen-glucose deprivation.

Conclusion: HFD-induced diabetes compromises the stemness of cerebral pericytes by altering p21–SOX2 signaling. These results provide evidence supporting the role of pericytes in diabetes-related CSVD and subsequent cerebral dysfunction.

Keywords

Pericyte, diabetes mellitus, cerebral small vessel disease, stemness

Introduction

Cerebral small vessel disease (CSVD), which commonly leads to lacunar strokes and vascular dementia,¹ can occur in association with diabetes, hypertension, smoking, radiation therapy, and genetic disorders.² Accumulating evidence is highlighting the increased burden of CSVD visualized by brain magnetic resonance imaging (MRI) of patients with type 2 diabetes mellitus.^{3,4}

In type 2 diabetes, microvascular complications can precede or progress simultaneously with the macrovascular complications.⁵ Regarding the particular involvement of cerebral small vessels in diabetes microangiopathy, pericytes, which localize around capillary or arteriolar walls, have been proposed to play crucial role on the pathogenesis.⁶ In patients with diabetes, pericyte loss is a pathological hallmark of diabetic retinopathy.⁷ Loss of cerebral pericytes is also observed in diabetes models.^{2,8–10} The central

nervous system (CNS) endothelium has significantly higher pericyte coverage than peripheral tissues,¹¹ suggesting that pericytes may have heightened functional

¹School of Medicine for International Students, I-Shou University, Kaohsiung

²Department of Neurosurgery, E-Da Hospital, I-Shou University, Kaohsiung

³Department of Surgery, National Cheng Kung University Hospital, College of Medicine, National Cheng Kung University, Tainan

⁴Department of Pharmacology, College of Medicine, National Cheng Kung University, Tainan

⁵Department of Neurology, National Cheng Kung University Hospital, College of Medicine, National Cheng Kung University, Tainan

⁶Department of Genomic Medicine, National Cheng Kung University Hospital, College of Medicine, National Cheng Kung University, Tainan

Corresponding author:

Yuan-Ting Sun, Department of Neurology, College of Medicine, National Cheng Kung University, No 1, University Road, Tainan 704, Taiwan.
Email: ytsun@mail.ncku.edu.tw



importance in the CNS. Pericytes cover most capillaries in the CNS and are uniquely positioned within the neurovascular unit to serve as vital integrators and effectors of multiple neurovascular functions, including angiogenesis, blood–brain barrier (BBB) maintenance, and neurovascular remodeling.^{12–15} The neurovascular unit is crucial for regeneration of brain tissue after a vascular insult.^{16–18} Pericytes typically change their phenotype in CNS injury to become proliferative and migratory and thus be recruited to the lesion sites.^{19,20} Moreover, pericytes are quiescent totipotent stem cells.²¹ Pericytes can be transformed into multipotent stem cells and differentiated into nonpericyte lineage cells, such as neural,²² microglial, and vascular cells.^{23–26} Both hypoxia²⁷ and ischemia can increase stemness of pericytes²⁵ through reprogramming.

Therefore, here, we hypothesize that type 2 diabetes impedes the postischemia regeneration process by compromising the ischemia-provoked pericyte dedifferentiation. To test the hypothesis, we adopt a high-fat diet (HFD)-induced non-insulin dependent form of diabetes mouse model, first described in 1988 and can recapitulate obesity, hyperinsulinemia, and altered glucose homeostasis as the patient phenotypes.^{28–31} Because the obesity is induced by environmental manipulation rather than by genes, it potentially models the human condition similarly to the real-world condition.^{28–31} With this HFD model, this study evaluated the effects of non-insulin dependent diabetes on the stemness of cerebral pericytes.

Methods

Mouse husbandry and HFD model

Animals were handled in strict accordance with the recommendations of the Guide for the Care and Use of Laboratory Animals of the National Institutes of Health. The protocol was approved by the Institutional Animal Care and Use Committee of National Cheng Kung University (Approval No. 107164), and the experiments were carried out in compliance with the Animal Research: Reporting of In Vivo Experiments guidelines.

Male C57BL/6N mice aged 8 weeks were purchased (BioLASCO Taiwan Co., Ltd, Taiwan) and randomly assigned to receive either a chow diet (Laboratory Autoclavable Rodent Diet 5010*; LabDiet, St. Louis, MO, USA) or a HFD (TestDiet-58Y1, 60% kcal from fat; TestDiet, St. Louis, MO, USA). The fat content of HFD was 34.9% (cholesterol, 301 ppm; linolenic acid (18:2), 4.7%; linolenic acid (18:3), 0.39%; arachidonic acid, 0.06%; omega-3 fatty acid, 0.39%; total saturated fatty acid, 13.68%; total monounsaturated fatty acid, 14%; total polyunsaturated fatty acid, 5.15%). The fat content of chow diet was 4.8% (cholesterol, 267 ppm; linoleic acid, 4.54%; linolenic acid, 0.13%; arachidonic acid, 0.02%; omega-3 fatty acid, 0.25%; total saturated fatty acid, 1.22%; total monounsaturated fatty acid, 1.2%). This *ad*

libitum diet was maintained for 12 weeks until the end of the experiment. Twelve weeks later, animals of each group went through either protocol shown in Figure 3(a) or 5(a).

Measurement of fasting levels of plasma glucose and insulin. After fasting, the mice were anesthetized with pentobarbital (0.1 g/kg, i.p.) and blood samples were collected from the orbital sinus with heparinized capillary tubes. Plasma was collected after centrifuging the blood at $3000 \times g$ for 10 min. Plasma glucose levels were determined by using a commercial glucose-oxidase kit (Cat. #: 11538, BioSystems, Barcelona, Spain). Plasma insulin levels were determined by using a commercial mouse insulin ELISA kit (Cat. #: 10-1247-01, Mercodia, Uppsala, Sweden).

Determination of insulin resistance. Insulin resistance was determined by using the homeostatic model assessment of insulin resistance (HOMA-IR = [glucose in mmol/L \times insulin in mU/L]/22.5)

Glucose tolerance test or insulin tolerance test. Glucose or insulin tolerance was determined using the glucometer Rightest GM700S (Bionime, Taichung, Taiwan) with blood samples obtained 15, 30, 60, 90, and 120 min after intraperitoneal injection of glucose (2 g/kg) or insulin (0.75 U/kg).

Distal middle cerebral artery occlusion surgery and 2,3,5-triphenyltetrazolium chloride stain

Mice were anesthetized using 1%–2% isoflurane in an atmosphere containing 30% oxygen (at 1–1.5 L/min) and placed on a thermostatically regulated heating pad set to 37°C. All surgical procedures were performed under the surgical microscope SteREO Discovery.V12 (Carl Zeiss Microscopy, Jena, Germany). To conduct distal middle cerebral artery occlusion (dMCAO), a unilateral temporal craniotomy was performed, and the ipsilateral MCA was permanently ligated at a point downstream from the lenticulostriate branches.³² To visualize the infarction region, mouse brain was isolated, placed into cold phosphate-buffered saline (PBS), and sectioned into serial 2-mm-thick coronal slices. Slices were immediately immersed in 1.5% 2,3,5-triphenyltetrazolium chloride (TTC; Merck, Darmstadt, Germany) dissolved in PBS, and incubated for 20 min at room temperature in the dark. After incubation, slices were washed and fixed with 3.7% paraformaldehyde for image capture.

Cerebral pericyte isolation

Mice were killed by CO₂ inhalation on poststroke day 3 according to nationally accepted protocols. Brain tissue samples were harvested immediately. The cerebellum and olfactory bulb were cut off. The postischemic area

containing leptomeninges was incubated with papain and DNase (Worthington Biochemical Corp., Lakewood, NJ) at 37°C for 70 min and then mechanically dissociated by passing through 19-gauge needles and then 21-gauge needles. After 22% bovine serum albumin was added, the mixture was centrifuged at 800–820 × *g* for 10 min to separate myelin. All cell studies were performed by investigators blinded to experimental group assignment.

Flow cytometry

Cells were stained with fluorescence-conjugated primary antibodies, anti-platelet-derived growth factor receptor β (PDGFR-β)-PE (1:50; Thermo Fisher Scientific, Waltham, MA, USA) and anti-neural/glia antigen 2 (NG2) (1:50; Merck Millipore, Darmstadt, Germany) for 30 min at room temperature. After washing, cells were sorted on a flow cytometer (FACSAria™ III, BD Biosciences, San Jose, CA, USA).

Sphere formation assay

Brain cells were grown in Gibco Dulbecco's modified Eagle's medium (DMEM)/F-12 medium (Thermo Fisher Scientific, Waltham, MA, USA) containing basic fibroblast growth factor (bFGF; 20 ng/mL), epidermal growth factor (EGF; 20 ng/mL; PeproTech, Rocky Hill, NJ, USA), 1% N-2 supplement (Thermo Fisher Scientific, Waltham, MA, USA), penicillin–streptomycin, and 2% fetal bovine serum for 1 week and moved into the low attachment dish (Alpha Plus Scientific, Taoyuan, Taiwan) with floating cultures at the density of 7–8 cells/μL in DMEM/F-12, EGF, fibroblast growth factor 2, and N-2 supplement for 21 days.²⁵ To treat the primary pericytes with p21 inhibitor, pericytes were incubated with 10 μM UC2288 (Abcam, Cambridge, UK) for 24 h before being grown in a suspension culture system. For a single experiment, at least four animals were required for the sphere forming assay.

Oxygen glucose deprivation

Pericytes isolated from non-ischemic mouse brain were washed twice with glucose deprivation medium composed of DMEM with no glucose and then incubated in a hypoxic chamber flushed with anoxic gas (95% N₂, 5% CO₂, and 1% O₂) for 3 or 24 h. After oxygen glucose deprivation (OGD), the medium was replaced with DMEM/F12 sphere media described above.

Immunofluorescence

Tissue samples for immunofluorescence were placed in optimal cutting temperature compound and then frozen in liquid nitrogen-cooled isopentane. Tissues in the thickness of 4 μm were incubated in the blocking serum (Thermo Fisher Scientific, Waltham, MA, USA) at room temperature

for 30 min, followed by incubation with primary antibody overnight at 4°C. The primary antibodies used in this study were rabbit anti-PDGFR-β (1:100; Abcam, Cambridge, UK), rabbit anti-NG2 (1:200; Merck Millipore, Darmstadt, Germany), rat anti-CD31 (1:50; GeneTex, Irvine, CA, USA), anti-glia fibrillary acidic protein (GFAP; 1:100; Cell Signaling Technology, Danvers, MA, USA), and rabbit anti-CD11b (1:100; BD Biosciences, San Jose, CA, USA) antibodies. The tissues were washed three times in PBS and then incubated for 1 h at room temperature with fluorescence-conjugated secondary antibodies Alexa Fluor 488-conjugated goat anti-rat immunoglobulin G (IgG, 1:200; Jackson ImmunoResearch Laboratories, West Grove, PA, USA) and Alexa Fluor 594 goat anti-rabbit IgG (1:200; Life Technologies, Carlsbad, CA, USA). The slides were mounted and examined under the FV1000 confocal microscope (Olympus, Tokyo, Japan). To quantify immunofluorescence intensity, all images were obtained at an equal setting in all optical parameters, such as exposure time, gain, and saturation. ImageJ (National Institutes of Health) was used for quantification. Averaged intensity was obtained and corrected with the background of each image.

Immunoblotting

Cells were homogenized in radioimmunoprecipitation assay lysis buffer with protease inhibitor cocktail (MilliporeSigma, Burlington, MA, USA) and phosphatase inhibitor cocktail (Abcam, Cambridge, UK), incubated for 30 min on ice, and centrifuged for 20 min at 14,000 × *g*. Protein (30 μg) was separated by 10% sodium dodecyl sulfate–polyacrylamide gel electrophoresis and subsequently transferred to nitrocellulose membrane (Bio-Rad Laboratories, Hercules, CA, USA). The protein was detected using primary antibodies: anti-p53, anti-p53 phospho-S15, and anti-p21 antibodies (Abcam, Cambridge, UK). The signal was detected by Western blotting with enhanced chemiluminescence substrate (Bio-Rad Laboratories, Hercules, CA, USA) according to the manufacturer's protocol.

Semiquantitative reverse transcription-polymerase chain reaction

RNA extraction was performed according to the instructions of the NucleoZOL RNA isolation kit (Macherey-Nagel, Düren, Germany), and complementary DNA (cDNA) was synthesized from RNA isolates with the RevertAid First Strand cDNA Synthesis Kit (Thermo Fisher Scientific, Waltham, MA, USA) according to the manufacturer's protocol. Polymerase chain reactions (PCRs) with one-tenth of the cDNA were carried out with OneTaq® DNA polymerase (New England Biolabs, Ipswich, MA, USA). The protocol was optimized for semiquantitative analysis.³³ In brief, the PCR procedures consisted of a denaturation step (94°C for 30 s), followed by 35

cycles of 94°C (30s), annealing temperature (30s), 68°C (30s), and a final extension step at 68°C for 5 min. PCR products were visualized through 1.5% agarose gel electrophoresis stained with SYBR Safe DNA Gel Stain (Thermo Fisher Scientific, Waltham, MA, USA). Information on PCR primer sequences and primer-specific annealing temperature is provided in Supplemental Table 1.

Detection of intracellular reactive oxygen species

Intracellular reactive oxygen species (ROS) were measured with DCFDA Cellular ROS Detection Assay kit (Abcam, Cambridge, MA, USA) on mouse cerebral pericyte treated with normal glucose (17.5 mM) or high glucose (30 mM) for 24 h. Cells were incubated with 25 μ M CM-H₂DCFDA for 45 min then the fluorescence intensity was determined by a microplate reader (Thermo, Fluoroskan, and Luminoskan Ascent). After subtracting the background intensity, which was obtained from a blank well with CM-H₂DCFDA and buffer only, all readouts were normalized to that of non-treatment control.

Statistical analysis

Values are presented as mean \pm standard deviation. After they passed the Kolmogorov–Smirnov normality test, data were compared using the paired or unpaired Student's *t* tests, one-sample *t* test, and two-way repeated measures analysis of variance (ANOVA) using Prism (version 6; GraphPad Software, La Jolla, CA, USA). Differences were considered significant at $p < 0.05$.

Results

HFD induces weight gain and systemic insulin resistance

To determine whether type 2 diabetes impaired the ischemia/hypoxia-provoked dedifferentiation and reprogramming of cerebral pericytes, the HFD-induced non-insulin dependent form of diabetes mouse model was adopted.³¹ After the mice were fed the HFD for 12 weeks, the mice gained significant body weight ($p < 0.0001$; Figure 1(a)–(c)) and presented with a significantly higher fasting glucose level ($p < 0.001$; Figure 1(d)), insulin level and HOMA-IR ($p < 0.0001$; Figure 1(e) and (f)). The glucose tolerance test and insulin tolerance test also demonstrated the development of insulin resistance in HFD mice ($p < 0.0001$; Figure 1(g), $p < 0.001$; Figure 1(h)).

Increase of cerebral pericytes after ischemic stroke

Cerebral pericytes usually increase in number after a cerebral ischemic event.³⁴ After dMCAO surgery, which

produces a more precise stroke volume in the brain,³⁵ the region of ischemia is clearly defined by TTC staining on poststroke day 3 (Figure 2(a)). In this corresponding region, cerebral pericytes labeled with unique markers, NG2 and PDGFR- β , were increased in number compared with the contralateral nonischemic region ($p = 0.0021$ in NG2 and 0.0017 in PDGFR- β , paired *t* test; Figure 2(b)–(d)). The stroke-provoked increment of cerebral pericyte was further quantified by flow cytometry on brain tissue using pericyte markers, PDGFR- β and NG2 (Figure 2(e) and (f)). On poststroke day 3, the count of PDGFR- β ⁺/NG2⁺ double positive cerebral pericytes increased threefold to fourfold ($p = 0.000574$; *t* test; Figure 2(g)).

Spheres formed from primary cerebral pericytes after ischemic stroke

Given the fact that a cerebral ischemic event can provoke the dedifferentiation process of cerebral pericytes,^{22–27} we isolated primary cerebral pericytes on the 3rd day after the ischemic stroke and performed a sphere-forming assay (Figure 3(a)), which is a simple approach for retrospectively identifying and quantifying cells that exhibit stem cell traits in multiple fields (e.g., cancer stem cell studies).³⁶ Culture methods used for inducing pericyte differentiation to neuronal, microglial, or vascular lineage cells were applied.^{24,25} The purity of cells was verified by staining with the molecular markers of pericytes (NG2 and PDGFR- β), endothelial cells (CD31), microglia (CD11b), and astrocyte (GFAP). The primary cerebral pericytes expressed NG2 and PDGFR- β , but not CD31, CD11b, and GFAP (Figure 3(b)). The expression levels of pericyte markers NG2, α -smooth muscle actin (α -SMA), and nestin from the chow- and HFD-fed groups were studied prior to sphere-forming assay, and no significant differences were observed ($p = 0.98$, 0.20, and 0.26 for NG2, nestin, and α -SMA, respectively; one-sample *t* test; Figure 3(c)). Then, equal numbers of pericytes from each group were moved to suspension culture dishes. Figure 3(d) shows an example of a pericyte-derived sphere. Compared the molecular markers between adherent pericytes prior to suspension culture and spheres from the same origin on day 21, the spheres showed reduced levels of pericyte markers (PDGFR- β , NG2, and α -SMA), increased levels of stem cell markers (sex-determining region Y box 2 (SOX2)), and increased levels of premature neuron markers (Tuj1; Figure 3(e)).

Reduced number and diameter of spheres in HFD group

After growing pericytes in the low attachment environment, the number of spheres was counted on days 14 and 21. In general, the sphere counts were reduced with time. HFD group-derived pericytes formed a smaller amount of spheres (Figure 3(f); two-way ANOVA for interaction,

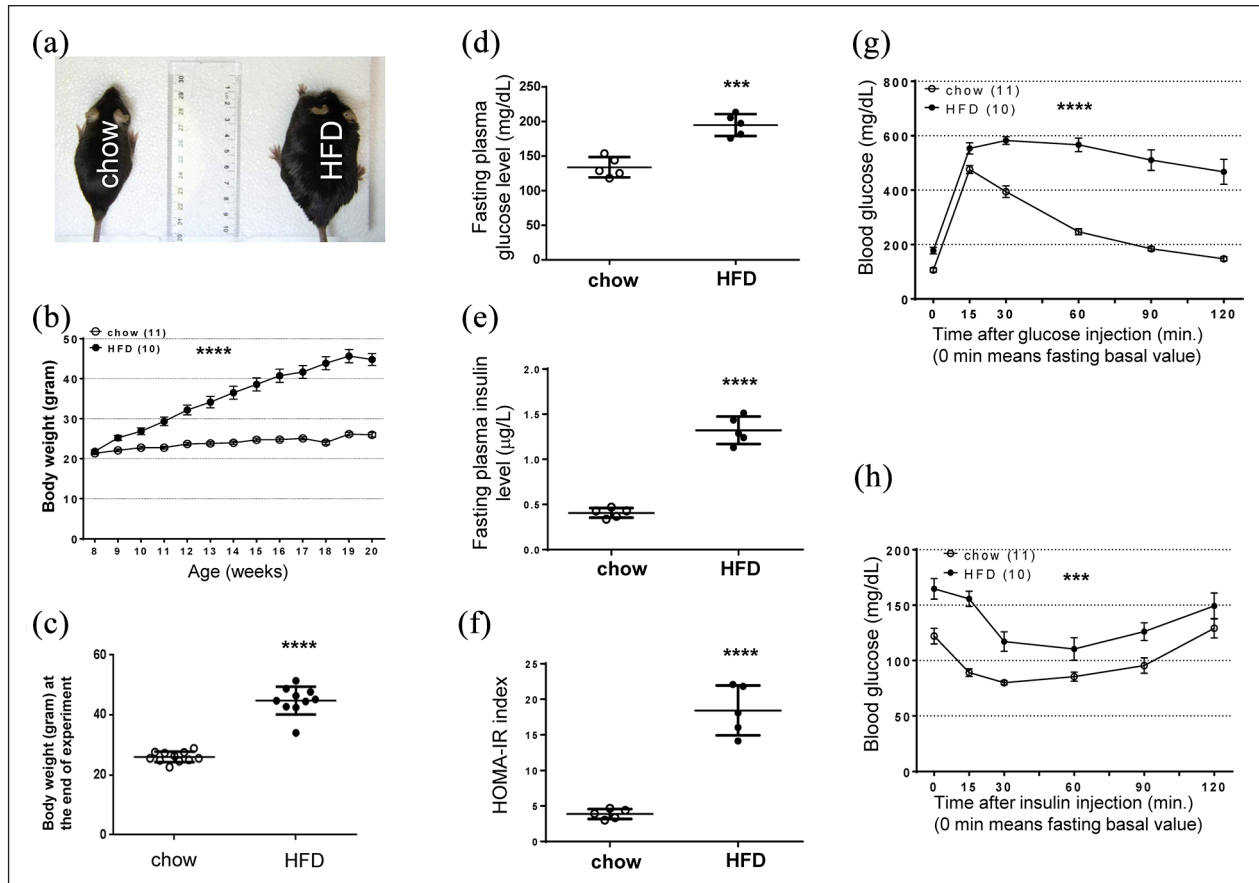


Figure 1. Effects of high-fat diet on body weight and systemic glucose metabolism: (a) representative photographs of the chow and high-fat diet (HFD)-fed mice, (b) weekly body weight of the chow ($n = 11$) and HFD ($n = 10$) groups, (c) a comparison of the final body weight after a 12-week treatment between chow ($n = 11$) and HFD ($n = 10$) groups, (d) fasting plasma glucose level, (e) fasting plasma insulin level, (f) homeostatic model assessment of insulin resistance which indicate insulin resistance, of the chow ($n = 5$) and HFD ($n = 5$) groups, (g) glucose tolerance was compared after fasted mice were challenged with 2g/kg glucose, and (h) insulin tolerance was compared after fasted mice were challenged with 0.75 U/kg insulin. Arrow at 0 min indicates the basal fasting glucose level before the injection of insulin. Chow group, $n = 11$; HFD group, $n = 10$. * $p < 0.05$, ** $p < 0.01$, *** $p < 0.001$, **** $p < 0.0001$, unpaired Student's t test for scatterplots, two-way repeated measures analysis of variance for the line graph. Numbers given in parentheses indicate the sample sizes.

$p = 0.023$; group factor, $p = 0.0019$; time factor, $p = 0.0086$), and the average sphere size was smaller than that in the chow group (chow and HFD groups, $130 \pm 47.7 \mu\text{m}$ and $76 \pm 28 \mu\text{m}$, respectively; $p < 0.0001$, unpaired t test; Figure 3(g)). Although the number of pericytes for the sphere-forming assay was equal in the two groups at the beginning, the HFD group showed a reduced amount of pericytes with ischemia-provoked stem cell traits. In addition, these cells in the HFD group showed less active proliferation and had a smaller sphere size.

Reduced markers of stemness in cerebral pericytes of HFD mice

After growing in suspension for 21 days, the level of pericyte marker NG2 was reduced in pericyte-derived spheres compared with that of adherent pericytes

($p = 0.016$ for comparison before and after sphere formation of a batch of pericytes by paired t test; Figure 4(a)), which suggested a dedifferentiation process.³⁷ However, this phenomenon was attenuated in the HFD group; the sphere/adherent ratio of NG2 was closer to 1 in the HFD group. Molecules relevant to stem cell signaling pathways, including YAP, SOX2, SMAD4, Notch3/DLL4, and β -catenin, were quantified and compared for pericytes before and after sphere-forming assay (Figure 4(b)). Comparing adherent pericytes with spheres, a 1.41-fold upregulation of SOX2 was found in the chow group, whereas an opposite response was found in the HFD group ($p = 0.0066$, paired t test; Figure 4(g)). In addition, a reduction of SMAD4 was found in the HFD group, whereas no change in SMAD4 level was noted in the chow group ($p = 0.018$, paired t test; Figure 4(f)). This indicated that the potential of

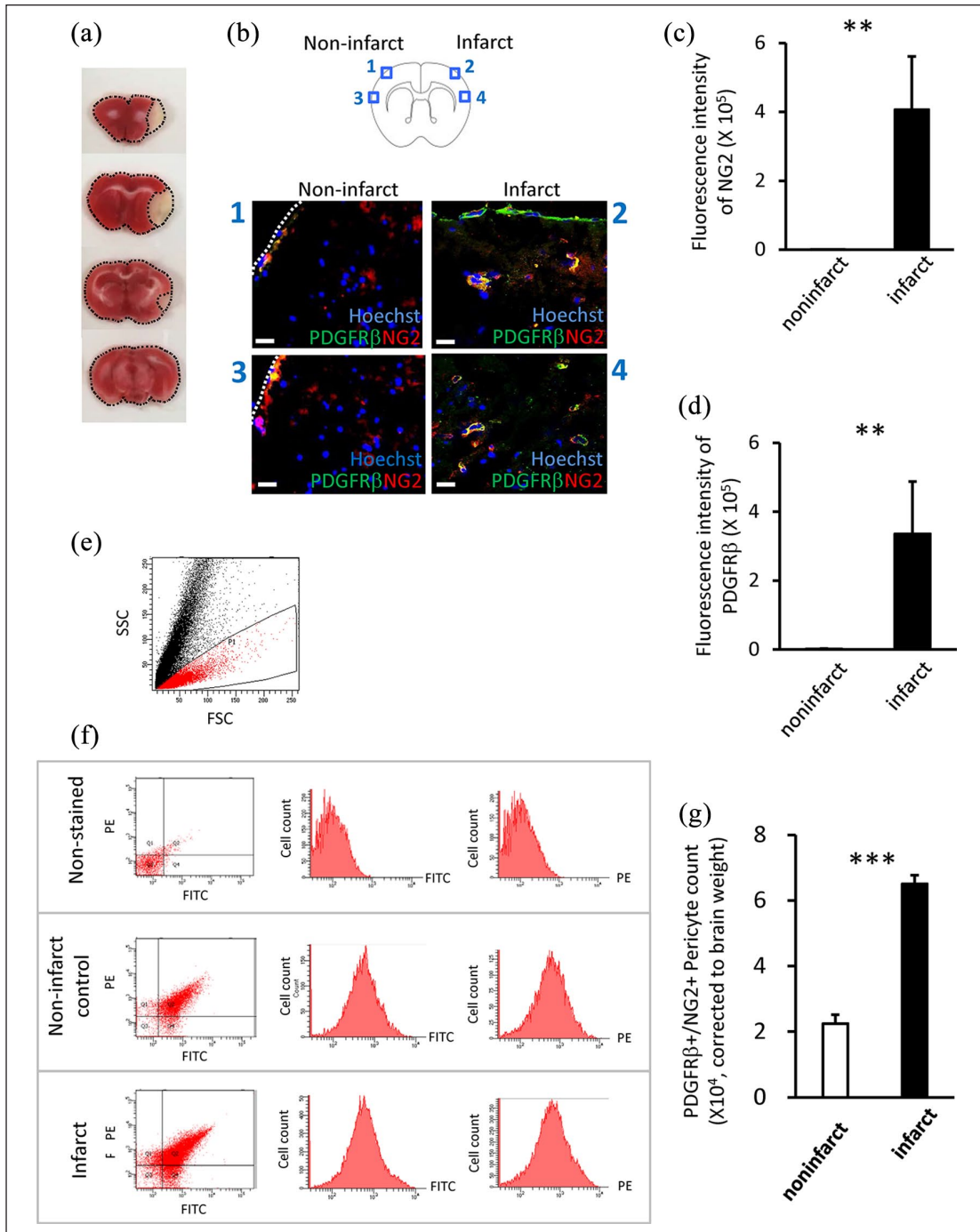


Figure 2. Cerebral ischemia provoked expansion of cerebral pericytes: (a) representative 2,3,5-triphenyltetrazolium chloride-stained coronal brain sections of one mouse on poststroke day 3 from six independent experiments ($n = 12$). The unstained area (white) is the region of infarction. From top to bottom, rostral to caudal, (b) representative images of immunofluorescence labeling of platelet-derived growth factor receptor- β (PDGFR- β) and neural/glial antigen 2 (NG2) on one mouse's brain from four independent experiments ($n = 8$). The 1–4 images were enlarged from the schematic blue box in the top. Scale bar = 50 μm , (c, d) a comparison of the quantified fluorescence intensity of NG2 (c) and PDGFR- β (d) between infarction and noninfarction areas. One pair indicates one animal. $n = 8$. Paired t test, (e) a representative dot plot showing population of brain cells. PDGFR- β^+ /NG2 $^+$ cerebral pericytes were mainly in the population in red, (f) representative dot plots and cell count graphs of flow cytometry from nine independent experiments. Top, non-stained control; middle and bottom, brain cells from noninfarct group (middle) and from infarct group (bottom) labeled with NG2-FITC and PDGFR- β -PE. x -axis, fluorescence intensity; y -axis, cell count, and (g) the count of PDGFR- β^+ /NG2 $^+$ pericytes from cerebral tissue by flow cytometry. y -axis, cell count, corrected with hemispheric brain weight of individual animal. Noninfarct group, $n = 9$; infarct group, $n = 7$. Unpaired t test. $p < 0.05$, $**p < 0.01$, $***p < 0.001$.

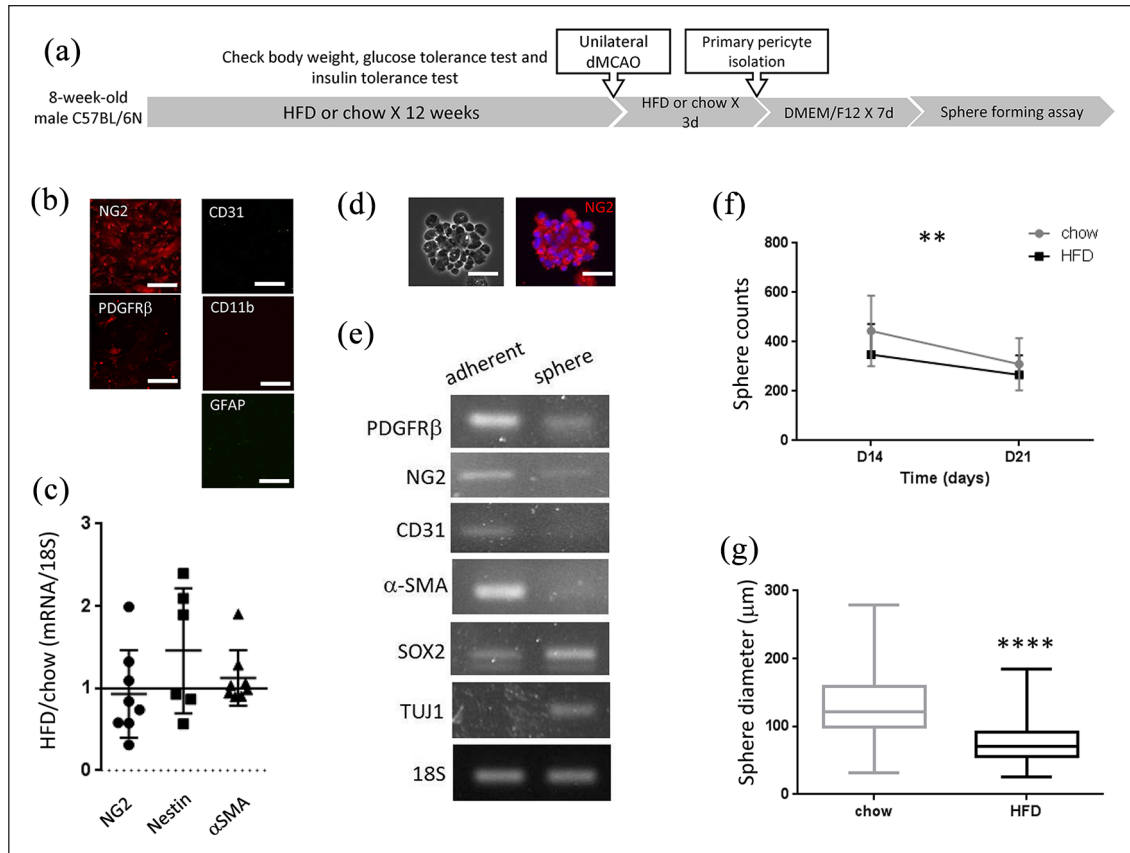


Figure 3. Sphere-forming assay from cerebral pericytes derived from postischemia brain: (a) schematic showing the time scale of the sphere-forming assay in poststroke high-fat diet (HFD) and chow groups, (b) representative images of immunofluorescence labeling showing the purity of primary cerebral pericytes from six independent experiments. Scale bar = 20 μm , (c) the ratio of the levels of pericyte markers on adherent pericytes from HFD and chow groups before sphere-forming assay. The mRNA levels of neural/glial antigen 2 (NG2), nestin, and α -smooth muscle actin (α -SMA) were determined by quantifying the intensity of gel bands and corrected with the levels of 18S. The ratio of HFD/chow was compared with one by one-sample *t* test. $n=8, 6,$ and 8 pairs for NG2, nestin, and α -SMA, respectively, (d) representative photographs of spheres derived from primary cerebral pericytes at day 21 from five independent experiments. Left: phase image; right: immunofluorescence image; blue: Hoechst; red: NG2. Scale bar = 50 μm , (e) representative RT-PCR results of multiple markers in adherent pericytes and spheres derived from the same origin at day 21 from five independent experiments, (f) comparison of sphere counts between HFD and chow groups. Every sample was counted at days 14 and 21. Statistics were calculated by two-way analysis of variance, and (g) comparison of sphere size between HFD and chow groups on day 21. Unpaired *t* test. $n=10$ independent experiments for each group. For a single experiment, at least four animals were required. $**p < 0.01$, $****p < 0.0001$.

dedifferentiation is reduced in cerebral pericytes derived from HFD mice.

Activation of p21 signaling in HFD mice attenuated ischemia-provoked dedifferentiation of pericytes

Given the fact that the expression levels of SOX2 were reduced in the spheres derived from HFD mice (Figure 4(g)), the upstream p53–p21 signaling pathway that regulates SOX2-mediated reprogramming was further studied.^{38,39} The levels of p53 and p21 in pericytes just before the sphere formation assay were determined (Figure 5(a) and (b)). Pericytes from the HFD group showed higher

levels of p21 and p53 ($p=0.008$ and 0.02 , respectively, unpaired *t* test; Figure 5(b)–(d)). In p21–SOX2 signal pathway, p21 and p53 usually suppress the downstream dedifferentiation signaling.^{40,41} Our results demonstrated that HFD mice-derived pericytes had a high level of p21, smaller amount of cells with stem cell trait and a low level of SOX2 in spheres. To further clarify the causal relationship of p21 in ischemia-provoked pericytes dedifferentiation, UC2288, a cell-permeable compound that selectively downregulates the expression of p21, was applied. After treating pericytes with 5 μM and 10 μM UC2288 for 24 h, the level of p21 was reduced, whereas the level of p53 was unchanged (Figure 5(e)). Adherent pericytes of the HFD group were incubated with 5 μM UC2288 for 24 h before

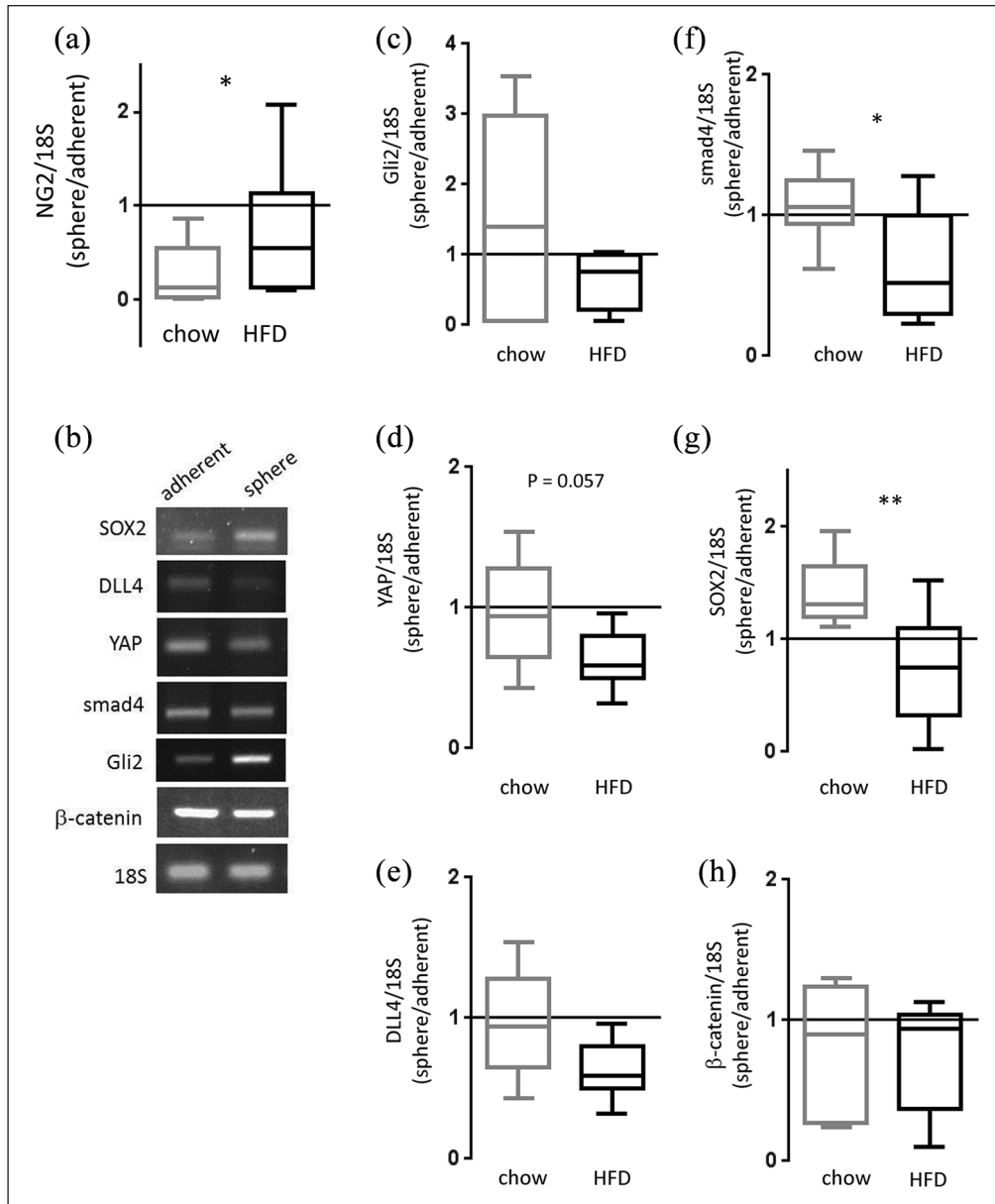


Figure 4. Quantified expression levels of stemness-related molecules before and after sphere formation: (a, c–h) comparisons of multiple markers before and after sphere formation. mRNA expression levels of pericyte marker neural/glia antigen 2 (NG2) (a) and stem cell markers Gli2 (c), YAP (d), DLL4 (e), SMAD4 (f), sex-determining region Y box 2 (SOX2) (g), and β -catenin (h). All quantified band intensities of reverse transcription-polymerase chain reaction gel were corrected with that of 18S. y-axis, ratio (spheres/adherent pericytes) of mRNA levels. $n=6-8$ independent experiments. At least four animals for a single group were used for one experiment. Comparison is before and after sphere formation of a batch of pericytes by paired t test. * $p < 0.05$, *** $p < 0.0001$. (b) Representative polymerase chain reaction gels of various stemness-related molecules in spheres and adherent pericytes.

the sphere formation assay (Figure 5(a)). After elimination of the elevated p21 by UC2288, the sphere number in the HFD group was rescued compared with the untreated HFD group ($p < 0.0001$, two-way ANOVA; Figure 5(f)). However, the average diameter of the spheres before and after the treatment was unchanged in both groups. The difference in diameter between the HFD and chow groups was not altered by the UC2288 treatment ($p < 0.0001$, two-way ANOVA; Figure 5(g)).

Hyperglycemia induced ROS provoked the following elevation of P21 and attenuation of SOX2 expression in post-ischemia sphere formation

To determine if the increase of p21 is caused by the chronic stress of hyperglycemia, ROS level was measured in cerebral pericytes grown in high glucose environment. After incubating pericytes in high glucose (30 μ M) medium for

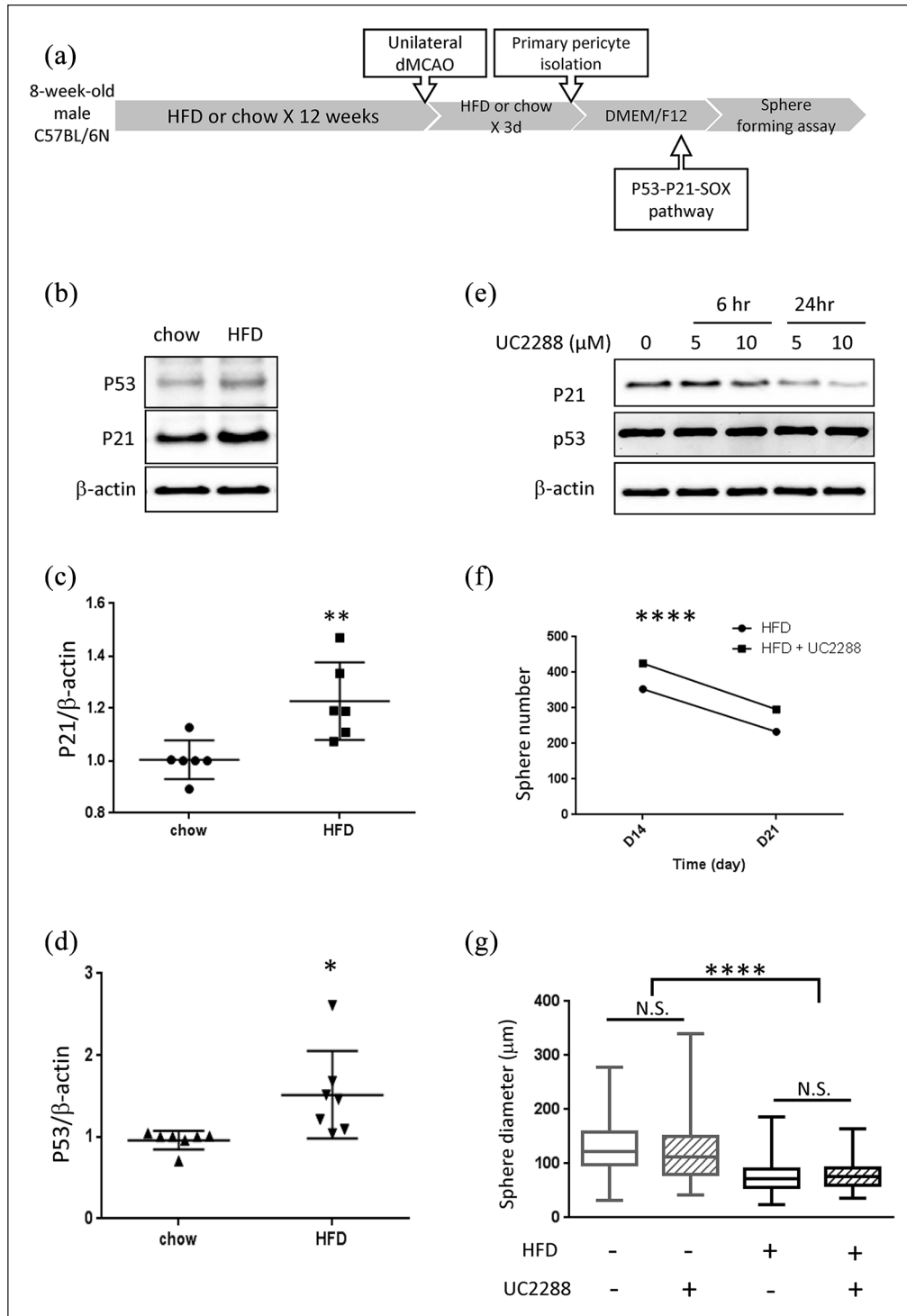


Figure 5. The role of p21 in posts ischemic dedifferentiation of cerebral pericytes: (a) schematic showing the time points of determining p21 and p53 levels, (b–d) representative immunoblot (b) and comparisons of quantified levels of p21 (c) and p53 (d) in pericytes derived from the high-fat diet (HFD) and chow groups before the sphere formation assay. The quantified protein levels were corrected with β -actin as an internal control. $n = 7$ independent experiments. At least four animals for each group were used in a single experiment. t test. (e) The levels of p21 and p53 in pericytes after incubating with various concentrations of UC2288 for 6 h or 24 h, (f, g) effect of UC2288 on sphere formation in the HFD group, (f) comparison of sphere number on day 14 and day 21 between untreated and UC2288-treated HFD groups. $N = 7$ independent experiments. At least four animals for each group were used in a single experiment. Two-way analysis of variance (ANOVA), and (g) comparison of averaged sphere size on day 21 between untreated and UC2288-treated HFD groups. One-way ANOVA. N.S.: not significant. * $p < 0.05$, ** $p < 0.01$, **** $p < 0.0001$.

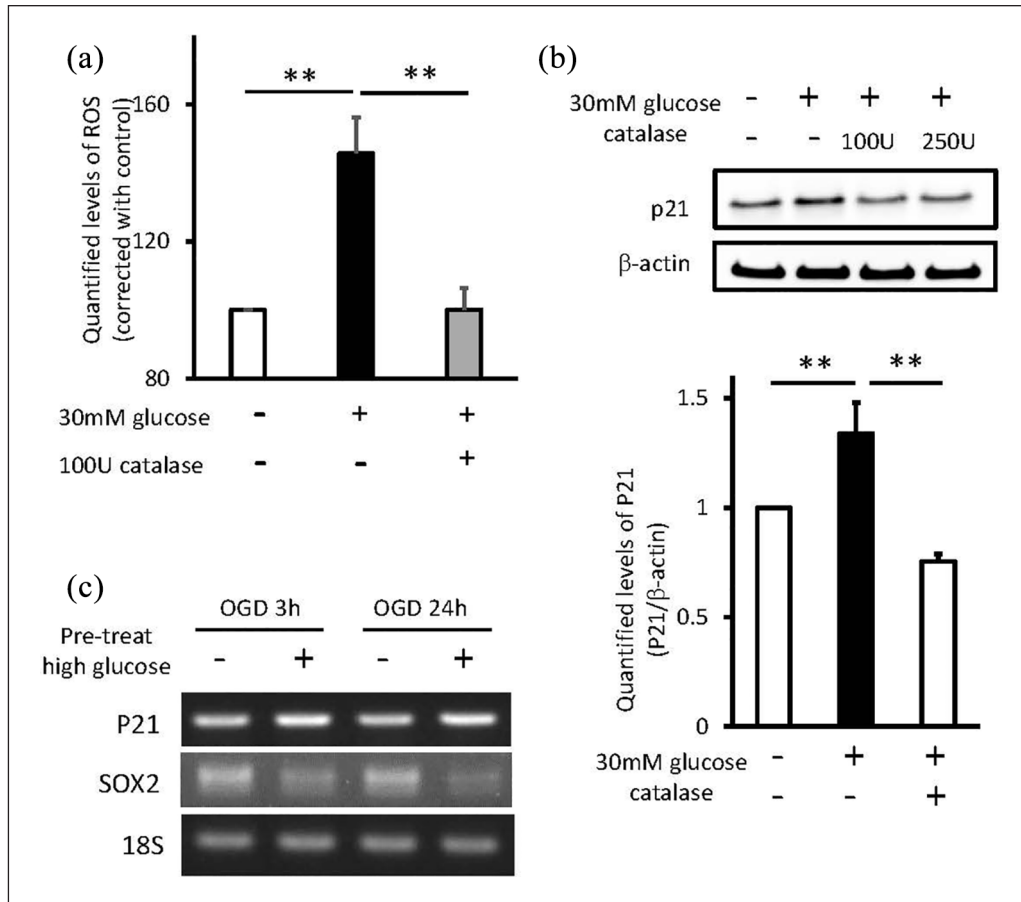


Figure 6. The hyperglycemia-induced ROS and the downstream P21–SOX2 signaling: (a) the quantified ROS levels in primary cerebral pericytes treated with high glucose or high glucose plus catalase. The ROS levels were corrected with non-treatment control. $N=6$ independent experiments, (b) levels of P21 in pericytes treated with high glucose or high glucose plus catalase. The quantified protein levels were corrected with β -actin as an internal control. $N=6$ independent experiments, and (c) the RNA levels of P21 and SOX2 in pericytes with or without high glucose pre-treatment, incubated in OGD chamber for 3 or 24 h. $N=4$ independent experiments. Unpaired t test, $**p < 0.01$.

24h, there was a 40% increase of ROS and elevated p21 protein levels comparing with control group (Figure 6(a)). While the ROS was abolished completely by catalase (Figure 6(a)), the high-glucose provoked increase of p21 was eliminated (Figure 6(b)). The hyperglycemia-treated pericytes were then undergone OGD for 3 or 24h. After OGD, SOX2 levels in pericyte were increased. However, the increase level was attenuated in pericytes pretreated with high glucose (Figure 6(c)). This clarified the signaling pathway from hyperglycemia to the subsequent reduction of ischemia-provoked pericyte sphere formation.

Discussion

This study demonstrated that HFD-induced hyperglycemia compromised the potential stemness of cerebral pericytes after ischemic stroke. First, after ischemic stroke, HFD group had a smaller number of spheres formed from an equal amount of cerebral pericytes compared with the chow group. Second, the expression levels of pericyte markers

decreased in parallel with the formation of the spheres in the chow group, but this was less prominent in the HFD group. Third, level of SOX2, a stemness-relevant molecule, increased with time in the spheres from chow group, whereas that was not noted in the HFD group. Fourth, HFD mice showed activation of the p21 signaling pathway, which can inhibit SOX2-mediated reprogramming, in cerebral pericytes before sphere formation. In addition, p21 signaling eliminated the number and the following expansion of pericytes with stem cell traits. Fifth, using a p21 inhibitor can rescue the dedifferentiation capability of cerebral pericytes derived from HFD mice. Sixth, at the cellular level, hyperglycemia induced an increase of ROS, which elevated the level of p21 and induced the subsequent phenomenon. The blockage of hyperglycemia-provoked ROS production, abolish the following increase of p21 level. These results demonstrated the stem cell trait of pericapillary cerebral pericytes. The potential of regeneration can be provoked in an ischemic event, but was compromised in HFD animal model through p21-mediated signaling.

The stem cell properties and the central location in neurovascular units make pericytes important for repair and regeneration after cerebral insults and make them a therapeutic target for preserving brain function in diabetes-related CSVD.⁴² In the process of regeneration, the stem cell niche provides a spectrum of cues that ensures plasticity of the stem cell compartment and prevents stem cell loss. In diabetes, multiple stress factors, such as oxidative stress, within the niche provide additional fine tuning of transcriptional programs, thereby compromising stem cell capability.^{43–46} Pericytes in close proximity to endothelial cells in brain microvessels are vital to the integrity of the BBB and are undoubtedly susceptible to oxidative stress.⁴⁷ Accordingly, this study demonstrated a reduced stem cell trait of cerebral pericytes in HFD-induced hyperglycemia model. The compromised dedifferentiation of pericytes may diminish postischemia neurovascular regeneration and may further lead to the suboptimal reestablishment of cerebral function. This finding provided one of the mechanisms by which patients with type 2 diabetes showed relatively worse poststroke outcomes or rapid declines of cognitive function in the real world.⁴⁸

Similar to that of other stem cells,^{49,50} SOX2 levels increased during the dedifferentiation process with pericyte sphere formation. However, the increase of SOX2 in pericytes from HFD mice was less than in the chow group. SOX2 is a transcription factor essential for maintaining self-renewal or pluripotency of undifferentiated stem cells and is negatively regulated by cyclin-dependent kinase inhibitor 1A (p21)⁴⁰ in neural stem cells,⁴¹ induced pluripotent stem cells,³⁹ and embryonic stem cells (ESCs).⁴⁰ Long-term exposure of ESCs to high glucose inhibits their proliferation by increasing oxidative stress and promoting increased expression and activity of the cell-cycle inhibitors p21^{Cip1} and p27^{Kip1}.⁵¹ The oxidative stress induced by hyperglycemia reduced the proliferation capability of stem cells.⁵¹ In the present study, we first demonstrated the involvement of p21 signaling in ischemia-provoked pericyte stemness. In HFD mice, the counts of pericytes with stem cell traits were reduced, and the proliferation of stem cells derived from pericytes (the sphere size) also declined. Although the p21 inhibitor rescued the sphere counts, it did not improve the sphere size (Figure 5(g)). That is, although the inhibition of p21 preserved the stem cell potential of pericytes, these pericytes from diabetes mice still showed an impaired proliferation capability. It is possible that HFD-induced hyperglycemia affects pericyte potency in two ways: one is by reducing the number of quiescent stem cells, and the other is by eliminating the stemness phenotype, including the proliferative capability and expression of signaling that drives the reprogramming.

Conclusion

Taken together, our results highlight the impact of type 2 diabetes in altering the potency of pericyte around cerebral

capillary and neurovascular units, which may further affect neurovascular regeneration after a vascular insult. This study provides evidence supporting the presence of progressive cerebral dysfunction in diabetes-related CSVD and the relatively worse clinical outcome of patients with diabetes after cerebral ischemia. Cerebral pericytes might possibly be a therapeutic target for diabetes-related CSVD.

Author contributions

YTS designed the experiments, analyzed the data, and wrote the manuscript. HKW, CYH, and YWC conducted the experiments and analyzed the data. All authors reviewed and approved the final version of the manuscript.

Declaration of conflicting interests

The author(s) declared no potential conflicts of interest with respect to the research, authorship, and/or publication of this article.

Funding

The author(s) disclosed receipt of the following financial support for the research, authorship, and/or publication of this article: This study was supported by Ministry of Science and Technology, Taiwan (MOST 109-2635-B-006-003).

ORCID iD

Yuan-Ting Sun  <https://orcid.org/0000-0003-2899-1136>

Supplemental material

Supplemental material for this article is available online.

References

1. Tan R, Traylor M, Rutten-Jacobs L, et al. New insights into mechanisms of small vessel disease stroke from genetics. *Clin Sci* 2017; 131: 515–531.
2. Ostergaard L, Engedal TS, Moreton F, et al. Cerebral small vessel disease: capillary pathways to stroke and cognitive decline. *J Cereb Blood Flow Metab* 2016; 36: 302–325.
3. Van Harten B, De Leeuw FE, Weinstein HC, et al. Brain imaging in patients with diabetes: a systematic review. *Diabetes Care* 2006; 29: 2539–2548.
4. Van Elderen SG, De Roos A, De Craen AJ, et al. Progression of brain atrophy and cognitive decline in diabetes mellitus: a 3-year follow-up. *Neurology* 2010; 75: 997–1002.
5. Chawla A, Chawla R and Jaggi S. Microvascular and macrovascular complications in diabetes mellitus: distinct or continuum? *Indian J Endocrinol Metab* 2016; 20: 546–551.
6. Winkler EA, Bell RD and Zlokovic BV. Central nervous system pericytes in health and disease. *Nat Neurosci* 2011; 14: 1398–1405.
7. Beltramo E and Porta M. Pericyte loss in diabetic retinopathy: mechanisms and consequences. *Curr Med Chem* 2013; 20: 3218–3225.
8. Junker U, Jaggi C, Bestetti G, et al. Basement membrane of hypothalamus and cortex capillaries from normotensive and spontaneously hypertensive rats with streptozotocin-induced diabetes. *Acta Neuropathol* 1985; 65: 202–208.

9. Price TO, Eranki V, Banks WA, et al. Topiramate treatment protects blood-brain barrier pericytes from hyperglycemia-induced oxidative damage in diabetic mice. *Endocrinology* 2012; 153: 362–372.
10. Shah GN, Morofuji Y, Banks WA, et al. High glucose-induced mitochondrial respiration and reactive oxygen species in mouse cerebral pericytes is reversed by pharmacological inhibition of mitochondrial carbonic anhydrases: implications for cerebral microvascular disease in diabetes. *Biochem Biophys Res Commun* 2013; 440: 354–358.
11. Shepro D and Morel NM. Pericyte physiology. *FASEB J* 1993; 7: 1031–1038.
12. Dore-Duffy P and LaManna JC. Physiologic angiodynamics in the brain. *Antioxid Redox Signal* 2007; 9: 1363–1371.
13. Sa-Pereira I, Brites D and Brito MA. Neurovascular unit: a focus on pericytes. *Mol Neurobiol* 2012; 45: 327–347.
14. Armulik A, Genove G, Mae M, et al. Pericytes regulate the blood-brain barrier. *Nature* 2010; 468: 557–561.
15. Fernandez-Klett F, Offenhauser N, Dirnagl U, et al. Pericytes in capillaries are contractile in vivo, but arterioles mediate functional hyperemia in the mouse brain. *Proc Natl Acad Sci USA* 2010; 107: 22290–22295.
16. Terasaki Y, Liu Y, Hayakawa K, et al. Mechanisms of neurovascular dysfunction in acute ischemic brain. *Curr Med Chem* 2014; 21: 2035–2042.
17. ElAli A. The implication of neurovascular unit signaling in controlling the subtle balance between injury and repair following ischemic stroke. *Neural Regen Res* 2016; 11: 914–915.
18. Huang L, Nakamura Y, Lo EH, et al. Astrocyte signaling in the neurovascular unit after central nervous system injury. *Int J Mol Sci* 2019; 20: 282.
19. Dore-Duffy P, Owen C, Balabanov R, et al. Pericyte migration from the vascular wall in response to traumatic brain injury. *Microvasc Res* 2000; 60: 55–69.
20. Zehendner CM, Sebastiani A, Hugonnet A, et al. Traumatic brain injury results in rapid pericyte loss followed by reactive pericytosis in the cerebral cortex. *Sci Rep* 2015; 5: 13497.
21. Dore-Duffy P, Katychev A, Wang X, et al. CNS microvascular pericytes exhibit multipotential stem cell activity. *J Cereb Blood Flow Metab* 2006; 26: 613–624.
22. Karow M, Camp JG, Falk S, et al. Direct pericyte-to-neuron reprogramming via unfolding of a neural stem cell-like program. *Nat Neurosci* 2018; 21: 932–940.
23. Dar A, Domev H, Ben-Yosef O, et al. Multipotent vasculogenic pericytes from human pluripotent stem cells promote recovery of murine ischemic limb. *Circulation* 2012; 125: 87–99.
24. Sakuma R, Kawahara M, Nakano-Doi A, et al. Brain pericytes serve as microglia-generating multipotent vascular stem cells following ischemic stroke. *J Neuroinflammation* 2016; 13: 57.
25. Nakagomi T, Kubo S, Nakano-Doi A, et al. Brain vascular pericytes following ischemia have multipotential stem cell activity to differentiate into neural and vascular lineage cells. *Stem Cells* 2015; 33: 1962–1974.
26. Karow M, Sanchez R, Schichor C, et al. Reprogramming of pericyte-derived cells of the adult human brain into induced neuronal cells. *Cell Stem Cell* 2012; 11: 471–476.
27. Mohyeldin A, Garzon-Muvdi T and Quinones-Hinojosa A. Oxygen in stem cell biology: a critical component of the stem cell niche. *Cell Stem Cell* 2010; 7: 150–161.
28. Surwit RS, Kuhn CM, Cochrane C, et al. Diet-induced type II diabetes in C57BL/6J mice. *Diabetes* 1988; 37: 1163–1167.
29. Winzell MS and Ahren B. The high-fat diet-fed mouse: a model for studying mechanisms and treatment of impaired glucose tolerance and type 2 diabetes. *Diabetes* 2004; 53(Suppl 3): S215–S219.
30. King AJ. The use of animal models in diabetes research. *Br J Pharmacol* 2012; 166: 877–894.
31. Heydemann A. An overview of murine high fat diet as a model for type 2 diabetes mellitus. *J Diabetes Res* 2016; 2016: 2902351.
32. Kuraoka M, Furuta T, Matsuwaki T, et al. Direct experimental occlusion of the distal middle cerebral artery induces high reproducibility of brain ischemia in mice. *Exp Anim* 2009; 58: 19–29.
33. Marone M, Mozzetti S, De Ritis D, et al. Semiquantitative RT-PCR analysis to assess the expression levels of multiple transcripts from the same sample. *Biol Proced Online* 2001; 3: 19–25.
34. Yang S, Jin H, Zhu Y, et al. Diverse functions and mechanisms of pericytes in ischemic stroke. *Curr Neuropharmacol* 2017; 15: 892–905.
35. Carmichael ST. Rodent models of focal stroke: size, mechanism, and purpose. *NeuroRx* 2005; 2: 396–409.
36. Pastrana E, Silva-Vargas V and Doetsch F. Eyes wide open: a critical review of sphere-formation as an assay for stem cells. *Cell Stem Cell* 2011; 8: 486–498.
37. Cai S, Fu XB and Sheng ZY. Dedifferentiation: a new approach in stem cell research. *Bioscience* 2007; 57: 655–662.
38. Wang LL, Su Z, Tai W, et al. The p53 pathway controls SOX2-mediated reprogramming in the adult mouse spinal cord. *Cell Rep* 2016; 17: 891–903.
39. Hong H, Takahashi K, Ichisaka T, et al. Suppression of induced pluripotent stem cell generation by the p53-p21 pathway. *Nature* 2009; 460: 1132–1135.
40. Ouyang J, Yu W, Liu J, et al. Cyclin-dependent kinase-mediated Sox2 phosphorylation enhances the ability of Sox2 to establish the pluripotent state. *J Biol Chem* 2015; 290: 22782–22794.
41. Marques-Torrejon MA, Porlan E, Banito A, et al. Cyclin-dependent kinase inhibitor p21 controls adult neural stem cell expansion by regulating Sox2 gene expression. *Cell Stem Cell* 2013; 12: 88–100.
42. Geranmayeh MH, Nourazarian A, Avci CB, et al. Stem cells as a promising tool for the restoration of brain neurovascular unit and angiogenic orientation. *Mol Neurobiol* 2017; 54: 7689–7705.
43. Hu Q, Khanna P, Ee Wong BS, et al. Oxidative stress promotes exit from the stem cell state and spontaneous neuronal differentiation. *Oncotarget* 2018; 9: 4223–4238.
44. Wang K, Zhang T, Dong Q, et al. Redox homeostasis: the linchpin in stem cell self-renewal and differentiation. *Cell Death Dis* 2013; 4: e537.
45. Bigarella CL, Liang R and Ghaffari S. Stem cells and the impact of ROS signaling. *Development* 2014; 141: 4206–4218.

46. Khacho M, Clark A, Svoboda DS, et al. Mitochondrial dynamics impacts stem cell identity and fate decisions by regulating a nuclear transcriptional program. *Cell Stem Cell* 2016; 19: 232–247.
47. Carvalho C and Moreira PI. Oxidative stress: a major player in cerebrovascular alterations associated to neurodegenerative events. *Front Physiol* 2018; 9: 806.
48. Sylaja PN, Pandian JD, Kaul S, et al. Ischemic stroke profile, risk factors, and outcomes in India: the Indo-US Collaborative Stroke Project. *Stroke* 2018; 49: 219–222.
49. Herreros-Villanueva M, Zhang JS, Koenig A, et al. SOX2 promotes dedifferentiation and imparts stem cell-like features to pancreatic cancer cells. *Oncogenesis* 2013; 2: e61.
50. Li Y, Adomat H, Guns ET, et al. Identification of a hematopoietic cell dedifferentiation-inducing factor. *J Cell Physiol* 2016; 231: 1350–1363.
51. Descalzo DLMC, Satoorian TS, Walker LM, et al. Glucose-induced oxidative stress reduces proliferation in embryonic stem cells via FOXO3A/ β -catenin-dependent transcription of p21(cip1). *Stem Cell Rep* 2016; 7: 55–68.